Model Simulation of Adiabatic Continuous Flow Stirred Tank Reactors

D. L. KEAIRNS and F. S. MANNING

Carnegie-Mellon University, Pittsburgh, Pennsylvania

Manning, Wolf, and Keairns' model for continuous flow-stirred tank reactors has been extended to include adiabatic as well as isothermal operation. The adiabatic, steady state yield of a continuous flow-stirred tank reactor was measured experimentally using the second-order, homogeneous, exothermic reaction between sodium thiosulfate and hydrogen peroxide. Model predictions of overall tank yield agreed closely with the data, thus verifying the applicability of this model to explain the effects of operating variables such as impeller size, impeller type, agitator speed, feed location, feed concentration, and flow rates.

Continuous flow-stired tank reactors (CFSTR) have received many theoretical and experimental studies. Their behavior is often described by simplified models because a complete theoretical analysis is prohibitively difficult. Design and analysis of a CFSTR are usually based on the assumption of complete isothermal mixing on a microscopic scale throughout the vessel. This simple model works surprisingly often, however experimental data indicate that this model does not hold for all operating conditions, especialy for low rev./min. and for viscous fluids (2, 4, 8, 9).

Manning, Wolf, and Keairns (3) proposed that a CFSTR be divided into two zones (Figure 1): 1. a small region engulfing and surrounding the impeller which is characterized by violent agitation, called a micromixer; and 2. the remaining tank volume where the mixing is comparatively mild, called a macromixer. The mixing in zone 1 is assumed to be perfect down to the molecular level. Fluid emanating from the impeller is assumed to undergo no micromixing during its recirculation throughout the vessel; that is, it behaves as if it were divided into completely segregated elements. All elements lose their identity whenever they pass through the impeller region. Usually the volume of the impeller region is approximately 1% of the total volume and thus the micromixer volume is neglected. The flow rate between the two zones depends on the impeller pumping capacity.

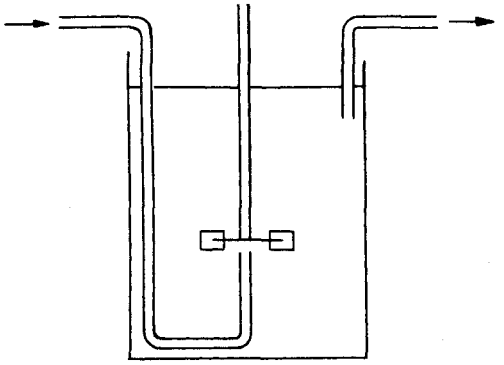

(A) PHYSICAL PICTURE

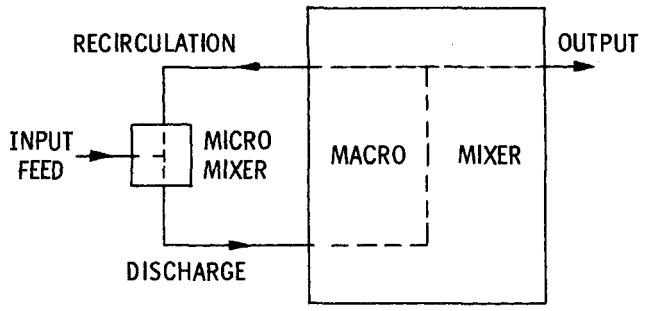

(B) FLOW AND MIXING PATTERNS

Fig. 1. Physical representation of micro-mixed feed model.

TABLE 1. MATERIAL BALANCE CONSIDERATIONS FOR IRREVERSIBLE SECOND-ORDER REACTION OF THE FORM

$$aA + bB \xrightarrow{k} \text{Products}$$

Operating Conditions	Micro Mixed Feed Model*
General R.T.D. General kinetics	$\overline{C}_o = \dfrac{QC_Q - FC_F}{Q - F}$ $\dfrac{\overline{C}_o}{C_Q} = \int_0^\infty \left(\dfrac{C_o}{C_Q}\right)_{\text{BATCH}} E(t)\,dt$
General R.T.D. Stoichiometric feed concentrations	$\left(\dfrac{C_o}{C_Q}\right)_{\text{BATCH}} = \dfrac{1}{1 + \dfrac{b}{a} kC_Q t}$
General R.T.D. Nonstoichiometric feed concentrations	$\left(\dfrac{C_o}{C_Q}\right)_{\text{BATCH}} = \dfrac{\Phi e^{-\Phi kt}}{\dfrac{b}{a}C_Q + \Phi - \dfrac{b}{a}C_Q e^{-\Phi kt}}$ $\Phi = C^B{}_Q - \dfrac{b}{a} C_Q$

* Concentration of component A represented by C. Concentration of component B represented by C^B.

This model has been applied previously to isothermal operation of a CFSTR (3); and it is now extended to the adiabatic case.

MODEL DESCRIPTION

This model assumes adiabatic, steady state operation, constant volume of liquid in the CFSTR, and low fluid viscosity thus permitting use of Wolf and Manning's correlations (7) of pumping capacity, that is, $Q = 2.3\,ND^2d$ for impellers, and $Q = 0.54\,ND^3$ for propellers.

Table 1 summarizes all equations based on material balances for the postulated flow and mixing patterns shown in Figure 1. Isothermal performance of the CFSTR can be predicted from these equations (3), but prediction of adiabatic operation requires the use of additional energy balances. The adiabatic temperature rise is readily computed from:

$$\Delta H(\overline{C}_o - C_F) = \rho\, c_p\, (\overline{T}_o - T_i) \qquad (1)$$

D. L. Keairns is with Westinghouse Electric Corporation, Research and Development Center, Pittsburgh, Pennsylvania, and F. S. Manning is at the University of Tulsa, Tulsa, Oklahoma.

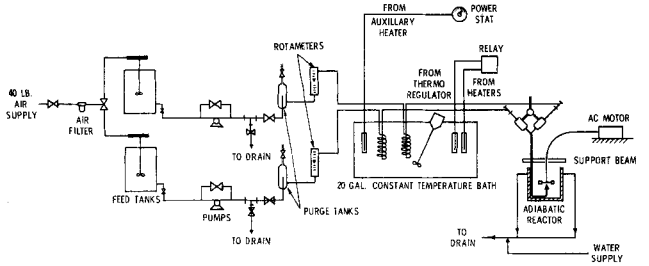

Fig. 2. Apparatus.

In fact much of the most recent and most accurate data (*1, 8*) on CFSTR have used the adiabatic temperature rise as a measure of conversion. It is incongruous to interpret conversion data based on adiabatic operation using an isothermal model. Variation of the reaction rate constant with temperature can be represented by an Arrhenius relationship.

$$k = k'e^{-E/RT_o} \tag{2}$$

Adiabatic reactor performance may now be predicted from Equations (1) and (2) and the material balance equations of Table 1. The resulting model predictions are represented very conveniently by the following dimensionless parameters:

Dimensionless concentration:

$$C_{DIM} = \frac{\overline{C_o} - C_{Plug}}{C_{Micro} - C_{Plug}} \tag{3}$$

where

$\overline{C_o}$ = outlet concentration based on adiabatic operation of proposed model.

C_{Micro} = outlet concentration based on adiabatic operation of a perfectly mixed CFSTR.

C_{Plug} = outlet concentration based on adiabatic operation of a plug flow reactor.

Dimensionless Flow Rate:

$$\frac{Q}{F} = \frac{\text{impeller discharge rate}}{\text{feed flow rate to reactor}} \tag{4}$$

Reaction Rate Modulus:

$$K = \frac{\tau}{\tau_{1/2}} = \frac{\text{mean holdup time}}{\text{reaction half-life}} \tag{5}$$

For the present second-order reaction considered with stoichiometric feed:

$$K = \frac{\tau}{\left(\frac{1}{2kC_F}\right)} = 2kC_F\tau \tag{6}$$

TABLE 2. KINETIC DATA

Sodium Thiosulfate-Hydrogen Peroxide Reaction (*3, 4*)

Reaction: $a\ Na_2S_2O_3 + b\ H_2O_2 \rightarrow$ products

Reaction order: second

Stoichiometric constant $= \frac{b}{a} = 2$

Heat of reaction $= \Delta H = -137 \frac{\text{k.cal}}{\text{mole}}$ $Na_2S_2O_3$ reacted based on stoichiometric feed data

$= -131 \frac{\text{k.cal}}{\text{mole}}$ $Na_2S_2O_3$ reacted based on 100% excess H_2O_2 data

Reaction rate constant $= k = 6.853 \times 10^{11}\ e^{-E/RT}$ $\frac{\text{liters}}{\text{g.-mole-sec.}}$ based on $\Delta H = -131 \frac{\text{k.cal}}{\text{g.-mole}}$

Activation energy $= E = 18{,}280 \frac{\text{cal.}}{\text{g.-mole}}$

EXPERIMENTAL METHOD

Of course any model examination requires accurate data. The second-order reaction between sodium thiosulfate and hydrogen peroxide was selected for intensive study toward testing the proposed model. While the mechanism of this reaction is not known, the overall description of the reaction and the rate law are consistent with that of a second-order reaction as indicated by Spencer's data (*5, 6*). The reaction is exothermic and the high heat of reaction results in non-isothermal operation. The relatively large adiabatic temperature rise thus provides a convenient method for measuring conversion. However, it has the disadvantage of producing temperature gradients in the reactor at low agitator speeds but this disadvantage is outweighed by the above advantages. Kinetics of the reaction are summarized in Table 2.

Equipment

A 2.79 liter reactor was chosen thus permitting study of the reactor performance over a wide conversion range without requiring inconvenient experimental restrictions on the volume of feed, temperature differences, or flow rates. Figure 2 is a schematic of the experimental apparatus, and the reactor, shown in Figure 3, was designed to be symmetrical and consistent with typical geometry. A 2 in., six-bladed impeller (diameter = 2 in., blade width = 0.469 in.) was used as the agitator for all runs. Rotational speed was continuously variable from 0 to 1,750 rev./min. and measured by using a hand tachometer.

Thermister probes were used to measure the inlet feed temperature and the reactor outlet temperatures. This method provided a technique for detecting temperature fluctuations less than 0.1°F. and thereby permitted measurement of the approach to steady state operation. The temperature probes could be adjusted to any desired depth or position in the reactor. The feed stream which entered the reactor through a 5 mm. I.D. glass tube, was introduced at one of three distinct locations as shown in Figure 4.

All the thermister probes were calibrated individually against two precision grade, mercury in glass thermometers by immersing the probes and the thermometers in a constant temperature water bath. Temperature comparisons were obtained over the entire operating range of operating temperatures, and the thermister probes were recalibrated after several runs. No drift was observed and therefore the initial thermister corrections were used; these corrections ranged from —0.1°F. to +0.1°F. with one probe requiring a 0.3°F. correction. All reported temperatures have been corrected using the appropriate term for the particular thermister.

Heat losses from the CFSTR were measured separately by filling the vessel with preheated, deionized water and observing the decrease in reactor temperature with time. These heat loss data were taken at impeller speeds of 0 to 310 rev./min., at initial reactor temperatures from 120 to 126°F., and for

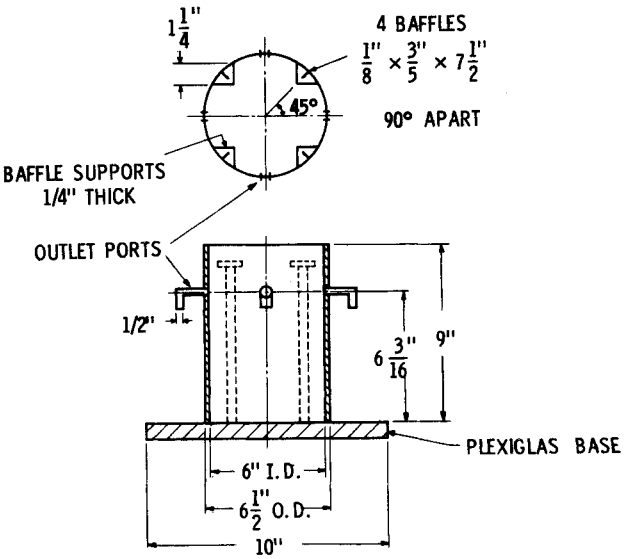

Fig. 3. Reactor dimensions.

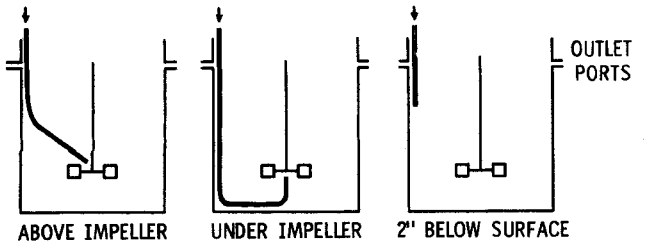

Fig. 4. Feed locations.

temperature measurements. Drift in the feed temperature was less than 0.01°F./min. A new agitator speed was selected and the system allowed to reach the new steady state. Details of the operating procedure are presented elsewhere (*1*).

EXPERIMENTAL RESULTS AND DISCUSSION

The scope of the present data is summarized in Table 3. Table 4 presents the data for a typical run (no. 24), while the method of calculating the reaction conversion from the raw data is indicated by appropriate footnotes in Table 4.

TABLE 3. SCOPE OF EXPERIMENTAL WORK

Feed location	Run No.	Reaction rate modulus	Outlet Temperature	Initial agitator speed	Data presented in figure
impeller region: above and below	18, 19, 20, 21, 22, 23, 24, 30, 32	16.5-28.2	average of 3 and 4 outlet ports	$N_i \leq 1{,}410$	5
under impeller	21, 22, 23, 24, 30, 32	17.6-23.5	average of 4 outlet ports (except run 21 where only 3 were recorded)	$N_i \leq 564$	6
2 in. below surface	26, 27, 28, and 31	16.1-20.3	average of 4 outlet ports	$N_i \leq 1{,}410$	7
above impeller	4 to 15, 18, 19, 20	18.4-32.5	runs 4 to 15: 1 port 18, 19, 20: 3 ports	$N_i \leq 615$	8

TABLE 4. EXPERIMENTAL RESULTS FOR RUN 24

Feed flow rate, F = 850 cc./min.
Inlet sodium thiosulfate concentration = 0.204 g.-moles/liter
Inlet hydrogen peroxide concentration = 0.408 g.-moles/liter

Run*	Impeller speed N, rev./min.	Feed temperature T_i, °F.	Average† outlet stream temperature $\overline{T_o}$, °F.	$Na_2S_2O_3$‡ outlet conc. $\overline{C_o}$, moles/liter	Dimensionless§ flow rate Q/F	Reaction‖ rate modulus K	Conversion %	C_{Dim}^{Exp}
24*a*	564	78.2	116.1	0.0433	46.9	17.6	78.8	1.003
24*b*	56	78.3	117.1	0.0395	4.7	18.5	80.7	0.900
24*c*	0	78.6	121.2	0.0233	1.0	22.7	88.6	0.455
24*d*	141	78.8	117.2	0.0412	11.7	16.8	79.8	0.964

* Data are reported in chronological order.

† The reported outlet stream temperature is the arithmetic average of separate steady state readings taken at the outlet ports. For example at 141 rev./min. the four individual port readings were: 117.3°F., 117.2°F., 117.0°F., 117.1°F.

‡ Compositions were computed from Equation (1): $\Delta H(\overline{C_o} - C_F) = \rho C_p(\overline{T_o} - T_i)$
where $\Delta H = -131$ k.cal./mole $Na_2S_2O_3$ reacted.

§ Impeller discharge, Q, was computed from Wolf and Manning's correlation (*7*)

$$Q = 2.3\ N\ D^2 d = 70.71\ N \text{ cc./min.}$$
$$Q = F \quad \text{for} \quad N = 0$$

‖ Reaction rate modulus $K = 2k\ C_F \tau$

$$\text{with } k = 6.853 \times 10^{11}\ e^{-(18280/(1.987)(\overline{T_o}))} \frac{\text{liters}}{\text{g.-mole-sec.}} \quad \text{where } \overline{T_o} = \text{°K.}$$

$$C_F = 0.204 \text{ moles/liter}$$

$$\tau = V/F = \frac{2.79 \text{ liters}}{0.850 \text{ liters/min.}} = 3.28 \text{ min.}$$

ambient temperatures from 77 to 84°F. All reported outlet temperatures have been corrected for these heat losses; these corrections were about 0.3°F. Details of the correction procedure are available (*1*).

Operating Procedure

Before each run 40 liters of 0.4 moles/liter sodium thiosulfate and 40 liters of 0.8 moles/liter hydrogen peroxide were prepared, analyzed, and placed in their respective feed tanks. As shown in Figure 3, during a run these reactant streams were passed through two calibrated rotameters, then through two coils submerged in the 20 gal. constant temperature bath, and finally mixed and introduced into the CFSTR via the 5 mm. I.D. glass tube. The constant temperature bath was controlled to ± 0.1°F., thus providing a constant feed temperature (about 80°F.) as it entered the CFSTR. An initial impeller speed was set and the reactant flow rates were kept constant until a constant outlet temperature was reached, usually within 10 min. Data for a given agitator speed were considered representative of steady state operation when the average corrected feed temperature varied less than 0.1°F. during the

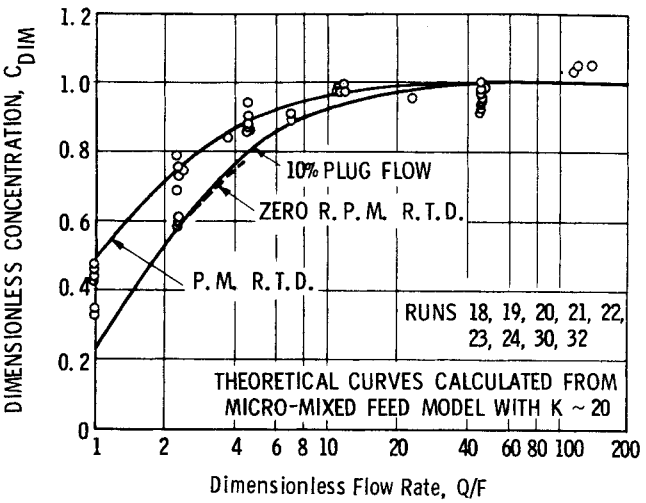

Fig. 5. Experimental data—feed introduced into impeller region.

Table 5 presents predictions arising from the adiabatic, micromixed model based on a perfectly mixed residence time distribution and run no. 24 conditions. Table 6 summarizes all runs and compares the data with the adiabatic micromixed model predictions based on a perfectly mixed residence time distribution.*

TABLE 5. ADIABATIC MODEL PREDICTIONS FOR RUN 24

Run	Predicted outlet stream temperature T_o, °F.	Predicted outlet concentration C_o g.-moles/liter	Predicted reaction rate modulus K	Conversion %	C_{Dim}^{Model}
24*a*	116.2	0.0430	17.7	78.9	0.996
24*b*	117.2	0.0389	18.6	80.9	0.884
24*c*	120.9	0.0246	22.3	88.0	0.489
24*d*	117.2	0.0412	18.6	79.8	0.966

Calculations of outlet temperature and concentrations involved the following trial and error techniques:

1. Assume an outlet stream temperature, T_o.
2. Assume an impeller discharge concentration, C_Q.
3. Evaluate the reaction rate constant, k.
4. Numerically evaluate $\int_0^\infty \left(\frac{C_o}{C_Q}\right)_{BATCH} E(t)\,dt$ and compute $\overline{C}_o$ (see Table 1).
5. Check C_Q assumption using material balance $FC_F + \overline{C}_o(Q - F) = C_Q Q$.
6. Repeat steps 2 to 5 until trial and computed values of C_Q converge.
7. Check T_o assumption using energy balance: $\rho C_p(T_o - T_i) = \Delta H(\overline{C}_o - C_F)$.
8. Repeat steps 1 to 7 until trial and computed values of T_o converge. Complete details are given elsewhere. (*1*).

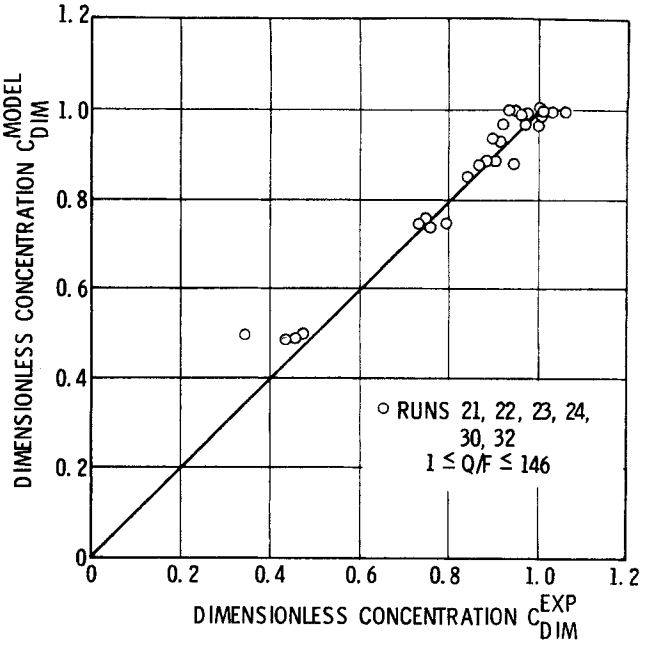

Fig. 6. Experimental vs. model predictions—feed under impeller.

Figure 5 presents the conversion data for runs where the feed was introduced into the impeller region. Because of the location of the feed inlet, feed bypass was considered unlikely and therefore the data were compared with the adiabatic model predictions based on perfect mixing, 10% plug flow, and Worrell's 0 rev./min. residence time distribution. At high impeller speeds, that is, at high impeller circulation rates or high Q/F, the three model predictions and the data all approached a dimensionless concentration of one. At these high recirculation rates, the reacting fluid within the vessel is recirculated through the impeller (and thereby micromixed) so frequently that the entire vessel behaves as a perfectly micromixed reactor. At intermediate rev./min. $2 < Q/F < 10$, the experimental data agreed with the adiabatic model based on a perfectly mixed residence time distribution; while at low rev./min. $Q/F < 2$, the data approached model predictions based on 10% plug flow or Worrell's residence time distribution. Of course reactor performance can be predicted more accurately if the actual residence time distribution is known *a priori*, but lacking such residence time distribution information, the adiabatic model with the two assumed residence time distribution brackets the data satisfactorily.

TABLE 7. SUMMARY OF RESIDENCE TIME DISTRIBUTIONS

Theoretical	
perfect mixing	$E(t) = \frac{1}{\tau} e^{-t/\tau}$
partial by-pass	$E(t) = \frac{(1-f)^2}{\tau} e^{-\frac{(1-f)t}{\tau}} + f\,\delta(t=0)$
partial plug flow	$E(t) = 0 \qquad 0 \leq t/\tau < P$
	$E(t) = \frac{1}{(1-P)\tau} e^{\frac{1}{1-P}(t/\tau - P)} \qquad t/\tau \geq P$
Experimental	
0 rev./min. R.T.D. (*8*)	$E(t) = 0 \qquad 0 < t < 0.06\tau$
	$E(t) = \left[14.643\frac{t}{\tau} - 0.87861\right]/\tau \qquad 0.06\tau < t < 0.13\tau$
	$E(t) = \frac{1.1845}{\tau} e^{-1.062\,t/\tau} \qquad t \geq 0.13\tau$

The data are now grouped according to the location of the feed inlet tube (c.f. scope of data in Table 3) and compared graphically with the adiabatic model predictions. All experimental data are compared with the adiabatic model predictions using the previously defined dimensionless concentration, flow rate, and reaction rate modulus. Calculation of model predictions requires a knowledge of the residence time distribution; and because experimental residence time distribution were not measured in the present work, model predictions were computed for the residence time distributions in Table 7.

Table 6 has been deposited as document NAPS-00486 with the ASIS National Auxiliary Publications Service, c/o CCM Information Sciences, Inc., 22 W. 34th St., New York 10001 and may be obtained for $1.00 for microfiche or $3.00 for photocopies.

Figure 6 presents data where the feed is introduced under the impeller, and the initial agitator speed was less than 565 rev./min. Predicted dimensionless concentrations, C_{DIM}^{model}, were calculated based on the respective experimental feed conditions assuming a perfect mixing residence time distribution. These data are in excellent agreement with the adiabatic micromixed model.

Figure 7 presents the data for runs where the feed was introduced far from the impeller. Predictions of the adiabatic micromixed feed model are consistent with the data if a small percentage of feed bypass is assumed to occur at low Q/F values; that is, low rev./min. While partial bypassing of the feed stream was not established by independent measurement, it is reasonable.

Figure 8 presents the data for runs where the feed was introduced above the impeller. Except for runs 18, 19, and 20; the outlet temperature was recorded at only one outlet port. Since subsequent runs indicate the temperature is not the same at each port, the data from runs 4 to 17 cannot easily be compared with the results where the feed was introduced under the impeller. However these data follow the trend predicted by the model, with considerable scatter about the 10% plug flow predictions.

At an agitator speed of 1,410 rev./min., the experimental dimensionless concentration were consistently larger than predictions from the model. This can be accounted for by a slight decrease in reactor volume at high agitator speeds. Intense foaming and pulse flow through the outlet ports were observed at 1,410 rev./min. which were not observed at lower agitation speeds. From a simulated static run using water, the volume remaining after mixing at 1,410 rev./min. was approximately 10% less than the volume after mixing at 564 rev./min. Decreasing the experimental volume by 7% reduced the dimensionless concentration so that it is consistent with the model predictions.

A detailed study of temperature profiles throughout the reactor was not made. Temperatures which were recorded near the impeller at 0 rev./min. were approximately 6°F. lower than the outlet temperature. Temperatures at high impeller speeds, large Q/F, were the same as the recorded outlet temperatures. These observations were consistent with the model which assumed that the temperature leaving the impeller region is a weighted average of the feed stream temperature and the recycle stream temperature.

CONCLUSIONS

As a result of this detailed comparison of the adiabatic micromixed model and the experimental data, these conclusions ensue:

1. The present model, which divides the CFSTR into a small micromixed impeller zone and a large macromixer,

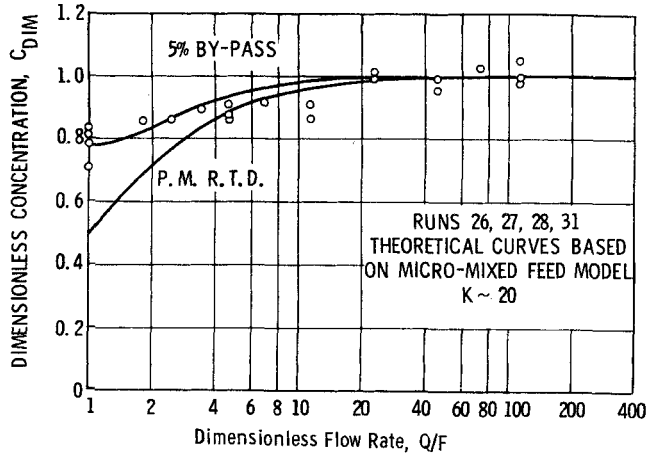

Fig. 7. Experimental data—feed introduced far from impeller.

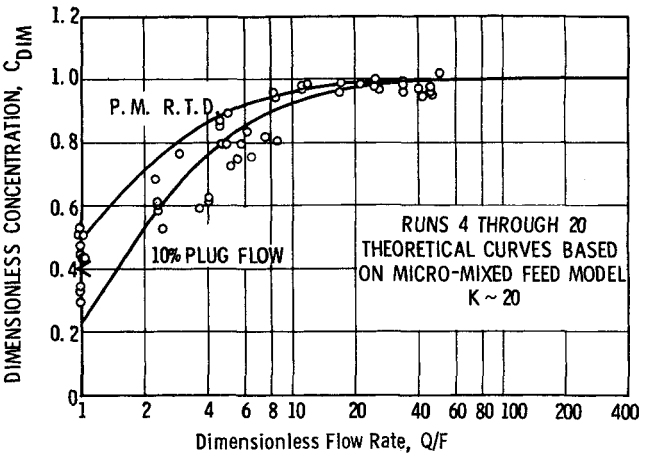

Fig. 8. Experimental—feed introduced above impeller.

may be used to simulate closely the adiabatic operation over all operating conditions.

2. This model requires only the following information: vessel size, impeller type size, rev./min., feed temperature and concentration. All of which are surely available to the design engineer.

3. Model predictions may be made more accurate if the assumed residence time distribution, perfect mixing which can be modified using a small amount of bypass or plug-flow, can be replaced by actual residence time distribution data.

4. At high rev./min., that is, when the impeller recirculation rate is at least twenty times the feed rate, both CFSTR yields and the model predictions approach that of a perfectly micromixed reactor.

5. At lower rev./min., the observed conversion differs from predictions based on complete, isothermal mixing down to the molecular scale throughout the vessel. These differences may be greater than 10%.

NOTATION

a = stoichiometric coefficient
b = stoichiometric coefficient
C = concentration of sodium thiosulfate
$\overline{C}$ = average concentration
C_F = feed concentration when it enters vessel
C_o = output stream concentration
C_Q = impeller discharge concentration when it leaves impeller
C_{micro} = output stream concentration when tank is perfectly mixed
C_{plug} = outlet concentration of a plug flow reactor
C_{DIM} = defined by Equation (3)
$C_{Na_2S_2O_3}$ = feed concentration of sodium thiosulfate
$C_{H_2O_2}$ = feed concentration of hydrogen peroxide
$\left(\frac{C_o}{C_i}\right)_{BATCH}$ = concentration variation with time in a completely micromixed, constant volume, batch reactor
c_p = heat capacity
D = impeller diameter
d = impeller blade width
E = activation energy
$E(t)$ = residence time distribution function
F = feed flow rate
f = fraction of feed stream that bypasses vessel without reacting
ΔH = heat of reaction
K = reaction rate modulus
k = reaction rate constant (for example, $k = k' e^{-E/RT_o}$)

N = impeller speed
N_i = initial impeller speed for given run
P = fraction of feed stream which undergoes plug flow
PMRTD = perfect mixing residence time distribution
Q = impeller discharge rate or impeller pumping capacity
R = gas constant
R.T.D. = residence time distribution
T = temperature
$\overline{T}$ = average temperature
T_i = inlet reactant temperature
T_o = reactor outlet temperature
t = time
V_T = volume of stirred tank
$\delta(t=0)$ = Dirac delta function
ρ = density
τ = mean holdup time in vessel
$\tau_{1/2}$ = reaction half time
Φ = defined in Table 1

LITERATURE CITED

1. Keairns, D. L., Ph.D. dissertation, Carnegie Inst. Tech., Pittsburgh, Pa. (1967).
2. LaRosa, P. and F. S. Manning, *Can. J. Chem. Eng.*, **42**, 65 (1964).
3. Manning, F. S., D. Wolf, and D. L. Keairns, *AIChE J.*, **11**, 723 (1965).
4. Ng, D. Y. C. and D. W. T. Rippm, Proc. Third European Symposium Chem. Reaction Eng., Amsterdam (Sept., 1964).
5. Spencer, J. L., Ph.D. dissertation, Univ. Pennsylvania (1961).
6. Spencer, J. L., and W. C. Cohen, *Chem. Eng. Progr.*, **58**, (12), 40 (1962).
7. Wolf, D. and F. S. Manning, *Can. J. Chem. Eng.*, **44**, 137 (1966).
8. Worrell, G. R., Ph.D. dissertation, Univ. Pennsylvania (1963).
9. Wu, D. T., Ph.D. dissertation, Mass. Inst. Tech., Cambridge (1962).

Manuscript received September 9, 1967; revision received April 26, 1968; paper accepted April 29, 1968. Paper presented at AIChE Tampa meeting.

Foaming and Frothing Related to System Physical Properties in a Small Perforated Plate Distillation Column

R. P. LOWRY and MATTHEW VAN WINKLE

The University of Texas, Austin, Texas

Experimental froth heights occurring on a perforated distillation tray were correlated with the determining system physical properties under distillation conditions. A photographic technique was used to measure accurately the foam and froth heights, produced in the 4 in. square test section of a laboratory distillation column, for several points in the composition range of five binary systems. Plate design parameters and operating vapor and liquid rates were held constant throughout the experimental study.

The froth height results from this investigation (11), as well as those from studies (17) of a 6 in. distillation column, show a linear relation with the expression, $U_A^2\ \rho V/(\rho L - \rho V)$, the frothing factor, for the ranges of the physical properties investigated.

The foam height results of this study indicate that the mass transfer surface tension gradient, the heat transfer gradient, and the absolute value of surface tension all contribute to foam formation and stability. Because of the complex relation between the surface tension gradient and the frothing factor in relation to the degree of foaming, as well as the effects of other influencing variables, a unique correlation of the foam height data resulting from mass transfer in this study was not feasible. However, it was possible to interpret quantitatively the nature of the effect for several of the data points.

This investigation was conducted to obtain experimental data which could provide a basis for correlation of the foam and froth heights occurring on an operating perforated distillation tray with system physical properties.

Depending on operating conditions and the system used, it is possible for either froth or foam to be formed on an operating distillation tray. Mukhlenov (*13*) and Pozin, et al. (*16*) describe froth as a vapor-liquid dispersion composed of small bubbles of vapor intermingled with streams of aerated liquid. Calderbank and Rennie (*4*) describe foam as comprised of large, cellular, relatively stable bubbles in close proximity.

The primary factor which determines whether froth or foam can be produced from a given liquid-vapor system is the ability of the liquid to form stable films as the vapor bubbles rise from the layer of liquid on a distillation tray into the space above. A system which exhibits this characteristic is generally referred to as a *foaming* system. A system which produces only froth on a distillation tray is usually called a *nonfoaming* system: Kitchener and Cooper (*8*) state that the property which distinguishes foaming from nonfoaming liquids is the ability to resist excessive localized thinning of a membrane (liquid film) while a controlled general thinning proceeds. This property is demonstrated in the effect of mass transfer on the surface tension of a film described by Zuiderweg and Harmens (*21*) and is characterized by the existence of surface tension gradients in the bubble laminae.

Vapor rate exerts an important influence on the nature of the vapor-liquid dispersion that actually occurs on a distillation tray. Several investigators (*2, 4, 12, 13, 15, 16, 18, 21*) have observed that low vapor rates favor the for-

R. P. Lowry is with the Celanese Chemical Company, Corpus Christi, Texas.